Supporting information for

Oxidase-like manganese oxides nanoparticles: A mechanism of organic acids/aldehydes as electron acceptors and potential application in cancer therapy

Yang Pan, [a] Zhuangzhuang Zhang, [a] Ju-E Cun, [a] Xi Fan, [a] Qingqing Pan, [b] Wenxia Gao, [c] Kui Luo, [d] Bin He [a,*] and Yuji Pu [a,*]

[a] National Engineering Research Center for Biomaterials, College of Biomedical Engineering, Sichuan University, Chengdu, 610064, China

[b] School of Preclinical Medicine, Chengdu University, Chengdu, 610106, China

[c] College of Chemistry & Materials Engineering, Wenzhou University, Wenzhou, 325027, China

[d] Huaxi MR Research Center (HMRRC), Department of Radiology, West China Hospital, Functional and molecular imaging Key Laboratory of Sichuan Province, Sichuan University, Chengdu, 610044, China

E-mail: bhe@scu.edu.cn (B. He); yjpu@scu.edu.cn (Y. Pu)

1 Materials

L-Histidine (His) was purchased from GL Biochem. Ltd. (Shanghai, China). $FeCl_3 \cdot 6H_2O$, $CuCl_2 \cdot 2H_2O$ and $Zn(NO_3)_2 \cdot 6H_2O$ were purchased from Chengdu Kelong Chemical Co. (China). $Mn(CH_3COO)_2 \cdot 4H_2O$ was purchased from Tianjing Damao Chemical Co. (China). Triethylamine (TEA), diphenylphosphoryl azide (DPPA), methylene blue (MB), 4,4'-diamino-3,3',5,5'-tetramethylbiphenyl (TMB), *o*-phenylenediamine (OPD), sodium ascorbate (NaA), 2,2'-azinobis-(3-ethylbenzthiazoline-6-sulphonate) (ABTS), indole 3-acetic acid (IAA), commercial MnO, MnO_2, Mn_2O_3, and Mn_3O_4 (MnO-c, MnO_2-c, Mn_2O_3-c, and Mn_3O_4-c) were purchased from Aladdin Bio-Chem Technology Co., Ltd. (Shanghai China). 1,3 Diphenylisobenzofuran (DPBF) was provided by J&K Scientific Co. Ltd (Beijing). Hydrogen peroxide was purchased from Chengdu Jinshan Chemical Reagent Co. Methylthiazoletetrazolium (MTT) and horseradish peroxidase (HRP) were provided by Sigma-Aldrich Co. Ltd. (Shanghai). The sodium D-isoascorbate (D-VC) and organic solvents were chemically pure and purchased from Chengdu Kelong Chemical Co. (China).

2. Experiments

2.1 Synthesis of poly(L-histidine) (PHis)

PHis was synthesized by a DPPA method according to previous studies.[1, 2] L-histidine (1.00 g, 6.45 mmol) were dispersed in anhydrous DMSO (2 mL) under N_2 atmosphere. TEA (2.06 mL, 14.8 mmol) and DPPA (1.8 mL, 8.4 mmol) were then added. The mixture was stirred in an ice bath for 2 h and then at room temperature for 2 d. After precipitation and centrifugation with ethyl ether (50 mL × 3), the residual crude product was dialyzed against ABS buffer solution (MWCO 1000, pH 5.0) for 2 h and ultrapure water for 4 h. PHis was obtained after freeze-drying (yield: 26%).

2.2 Preparation of Mn_3O_4 and PHis-coated metal oxide nanoparticles (PHis-M)

For the synthesis of PHis-Mn, PHis solution in DMF (1.37 mg /mL, 2 mL) and 50 μL TFA were added into $Mn(CH_3COO)_2 \cdot 4H_2O$ solution in DMF (2.45 mg/mL, 2 mL). After stirring for 1 min, 50 μL of NaOH aqueous solution (1 M) was added to adjust the pH to about 7. The product was collected after centrifugation and washing with water. The products with different metals and concentrations ratio were prepared similarly. Mn_3O_4 was synthesized similarly except using water as solvents and without adding PHis and TFA. Other transition metal oxide-based NPs (PHis-M, M= Fe, Cu and Zn) were prepared similarly.[3-6]

2.3 Characterizations

^{1}H NMR spectra were recorded with a Bruker Avance III 400 MHz NMR spectrometer and the solvents were TFA-*d*. The molecular weight of PHis was measured using Bruker AutoFlex III Mass Spectrometer. Fourier-transform infrared spectroscopy (FT-IR, Thermo a Nicolet AVATAR 360, New York, USA) was used to explore the chemical functionalities of samples by the KBr pellet method. A laser confocal Raman spectrometer (LabRAM HR, HORIBA, France) was also used to test the molecular structures of samples (λ = 532 nm). X-ray diffraction (XRD) was implemented to obtain the crystalline patterns of the material by scanning the powdered sample in the 2θ range of 15-75° at a 5°/min scanning speed (λ = 1.54 Å). X-ray photoelectron spectroscopy (XPS, AXIS Ultra DLD) was used to measure the crystal structure and surface valence of the PHis-Mn and Mn_3O_4. Dynamic light scattering spectrometer (DLS, Malvern Zetasizer Nano ZS) was employed to characterize the diameters. The morphology and distribution of PHis-Mn and Mn_3O_4 were obtained by a scanning electron microscope (SEM, S4800, Hitachi Ltd., Tokyo, Japan), transmission electron microscopy (TEM). Inductively coupled plasma optical emission

spectrometer (ICP-OES) was used to record metal ion weights of the samples.

2.4 The influence of H_2O_2

PHis-Mn was dispersed in ABS (pH 5.5 or 7.4 was be regulated by HCl or NaOH, 0.4 mg/mL, 200 μL) and then 200 μL of H_2O_2 (400 μM) were mixed with the dispersion and shaken for 30 min. Finally, 4 μL of TMB was added to test absorbance. The absorbance of the TMB was recorded by microplate reader. Add 100 μL of the mixture per well.

2.5 Catalytic mechanism of PHis-Mn

Exploration the reaction products of PHis-Mn and TMB. The gas chromatography (GC, Agilent 7890B, USA) was used to analysis the product of PHis-Mn. The PHis-Mn (0.5 mg/mL) and TMB (1.2 mM or 3.6 mM) were mixed into sodium acetate buffer (0.1 M, pH 5.5) and incubated for night. Then the supernatant was obtained and analyzed by gas chromatography with a headspace injection mode.

Exploration the effects of aldehydes, acids and alcohols on the catalytic performance of PHis-Mn. PHis-Mn (70 μg/mL), TMB (0.8 mM) and each kind of aldehydes (10 mM) were mixed into water (500 μL). The absorption of TMB was measured by UV spectrometer. The influence of acids and alcohols were used the same method as above. The aqueous solution was adjusted to pH 5.5 by HCl or NaOH. The effects of different kind of alcohols, aldehydes and acids on the catalytic performance of MnO_2-c, Mn_2O_3-c, Mn_3O_4-c, MnO-c was tested similarly.

2.6 Catalytic kinetic parameters of PHis-Mn and Mn_3O_4

To determine the initial rate of the reaction, Michaelis-Menten plot of Catalytic activity according to the variation concentration of TMB (0, 40, 80, 160, 240 and 320 μM) were reacted with 70 μg/mL of PHis-Mn (or Mn_3O_4) in NaAc-HAc buffer solution (pH = 5.5) (ε = 39000/(M·cm) for TMB).The

kinetic parameters (K_m and V_{max}) were calculated by the Michaelis-Menten Eq. (1). The Michaelis-Menten constant and the maximal reaction rate could be calculated by depicting Lineweaver-Burk plot. The formula of Lineweaver-Burk plot is as follows Eq. (2):

$$V = (V_{max} \times [S]) / (K_m + [S]) \quad (1)$$

$$1/V = (K_m + [S])/V_{max}[S] = 1/V_{max} + K_m/V_{max} \times 1/[S] \quad (2)$$

, where K_m is the Michaelis-Menten constant, V_{max} is the initial maximum reaction velocity, V is the initial reaction velocity, and [S] is the different concentration of substrate concentration.

2.7 TMB oxidation experiment under different pH and solution

The PHis-Mn was added to sodium acetate buffer solution (0.1 M pH 1.0-8.0) and HCl solution (pH 1.0-8.0) containing 0.5 mM TMB (pH was adjusted by HCl or NaOH). The absorption at 650 nm was measured.

2.8 Catalytic effect of different substrates

PHis-Mn (70 μg/mL) mixed with TMB (0.8 mM) into the solution (500 μL, pH 5.5 water or ABS) with or within H_2O_2 (100 mM, 4 μL). The UV-vis absorption spectra were recorded after 10 min of reaction by a microplate reader. Other substrates including ABTS (5 mM), OPD (0.16 mM), MB (22 μM) and NaA (0.8 mM) were tested in the same condition.

2.9 Computational details

Spin-polarized first-principle calculations were performed by the density functional theory (DFT) using the Vienna Ab-initio Simulation Package (VASP) package.[7] The generalized gradient approximation (GGA) with the Perdew-Burke-Ernzerhof (PBE) functional were used to describe the electronic exchange and correlation effects.[8-10] Uniform G-centered k-points meshes with a resolution of 2π*0.04 $Å^{-1}$ and Methfessel-Paxton electronic smearing were adopted for the integration in the Brillouin zone for geometric optimization. Boundary conditions were periodic in the x and y directions and surfaces were separated by 15 Å of vacuum in the z direction. The simulation was run with a cutoff energy of 500 eV throughout the computations. These settings

ensure convergence of the total energies to within 10 meV per atom. Structure relaxation proceeded until all forces on atoms were less than 10 meV $Å^{-1}$ and the total stress tensor was within 0.03 GPa of the target value. The DFT+U approach[11] was used to modify the intra-atomic Coulomb interaction among strongly correlated Mn 3d electrons. In the calculations, we applied $U_{eff} = 4$ eV for Mn 3d electrons.

The Gibbs free energy change (ΔG) of intermediates process was calculated by using the computational hydrogen electrode (CHE) model proposed by Nørskov et al.[12] The elementary steps of CH_3COOH reduction in the free energy profiles calculation are as follows:

(i) $CH_3COOH^* + H^+ + e^- = CH_3CO^* + H_2O$

(ii) $CH_3CO^* + H^+ + e^- = CH_3CHO^* / CH_3CHO$

(iii) $CH_3CHO^* + H^+ + e^- = CH_3CH_2O^*$

(iv) $CH_3CH_2O^* + H^+ + e^- = CH_3CH_2OH$

The asterisk (*) indicates the adsorption sites on the material surface. Then, the ΔG value can be determined as follows Eq. (3):

$$\Delta G = \Delta E + \Delta E_{ZPE} - T\Delta S \quad (3)$$

, where ΔE is the electronic energy difference directly obtained from DFT calculations, ΔE_{ZPE} is the change in zero-point energies, T is the temperature (298.15 K), and ΔS is the entropy change. The zero-point energies and entropies of the adsorption species were computed from the vibrational frequencies, in which only the adsorbate vibrational modes were calculated explicitly, while the catalyst sheet was fixed.

2.10 The IAA or PHis-Mn concentration dependence of DPBF consumption

The IAA concentration dependence: PHis-Mn (14 μg/mL) and different concentration of IAA (0-1 mM) were mixed with DPBF (50 μM) for 10 min. The PHis-Mn concentration dependence: different concentration of PHis-Mn (0, 5.6, 11.2, 16.8, 22.4, 28 μg/mL) and IAA (500 μM) were mixture with DPBF (50 μM) for 10 min. The absorbance was measure by UV-Vis spectrograph.

2.11 The comparison of catalytic effect between HRP and PHis-Mn

The same concentration of HRP and PHis-Mn (14 μg/mL) was added respectively into water

with IAA (500 μM) and DPBF (50 μM). The absorbance was recorded within 10 minutes.

2.12 The catalytic effect of PHis-Mn on IAA

TMB oxidation reaction. The catalyst PHis-Mn (7 mg/mL, 5 μL), IAA (20 mg/mL, 5 μL) and TMB (80 mM, 5 μL) were added into ultrapure water (500 μL). The absorption was measured by UV spectrometer after 10 min.

The detection of radical species. DPBF can be used to measure many kind of radical species [13]. The reaction between DPBF and radical species will cause the decrease in absorbance of DPBF. PHis-Mn (14 μg/mL) and IAA were mixture with DPBF (50 μM) for 10 min. Then the absorbance was measure by UV-Vis spectrograph.

Intracellular ROS was still detected by DPBF. After incubated with PHis-Mn (50μg/ml), IAA (4mM) and D-VC (0.5mM) for 8 h, 4T1 cells were stained with DPBF (100 μM) for 30 min. The fluorescence intensity of cells was measured by confocal laser scanning microscopy (CLSM) with emission (560 - 520 nm) with excitation at 405 nm.

Cell cytotoxicity. 4T1 breast cancer cells were used to test cell cytotoxicity by an MTT method. Cells were inoculated in 96-well plates at the density of 5×10^3 cells/well. After 24 h, the culture medium include PHis-Mn (50 μg/mL) firstly incubated for 4 h and then different concentrations of IAA (0.125 - 4 mM) were treated with cells for another 48 h. The cells treated with IAA or PHis-Mn only were set as the control. After then, the absorbance at the wavelength of 570 nm was measured by microplate reader, and the results were expressed as average ± SD (n = 5). The ROS scavenging experiment was similar to above, just adding different concentration of D-VC at the same time as IAA.

2.13 Statistical analysis

All data are presented as mean ± SD. The statistical significance of difference between groups used one way (ANOVA), unpaired *t*-test, and two-tailed unpaired Student's t-test to assess. Statistical significance of the text, figures and legends were defined as $*p < 0.05$, $** p < 0.01$ and $*** p < 0.001$.

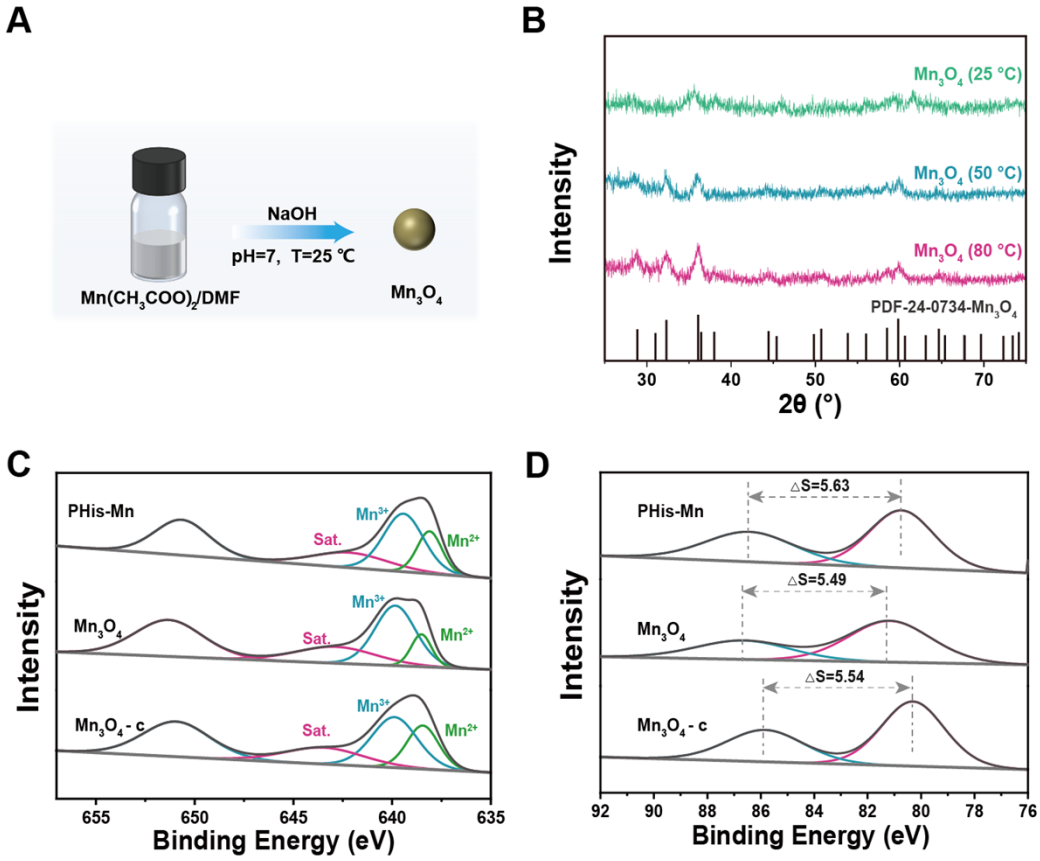

Figure S1. (A) Synthesis of Mn_3O_4 NPs. (B) PXRD patterns of Mn_3O_4 prepared at 25, 50, and 80 °C. (C) Mn 2p and (D) Mn 3s XPS spectra of Mn_3O_4, Mn_3O_4-c and PHis-Mn.

The crystalline structure was identified as Mn_3O_4 by powder X-ray diffraction (PXRD) results (Figure S1B), where the crystallinity of Mn_3O_4 NPs was improved at an elevated temperature. XPS analysis further confirmed the identity of Mn_3O_4 (Figure S1C, S1D and S2). The average oxidation state (AOS) of Mn was tested according to the following equation (4):[14]

$$AOS=8.95-1.13\ \Delta S \qquad (4)$$

, where ΔS is the multiple splitting of Mn 3s peak. Thus, the AOS of Mn in Mn_3O_4 was 2.75, close to that of commercial Mn_3O_4 (Mn_3O_4-c). The Mn_3O_4 used in this study was prepared at 25 °C if not indicated. In the Raman and FTIR spectra (Figure S3), the skeletal vibrations, deformation modes of the Mn-O-Mn chains in the octahedral lattice and stretching modes of the Mn-O bonds in MnO_6 octahedra were detected [15-17]. These all indicated the successful preparation of Mn_3O_4.

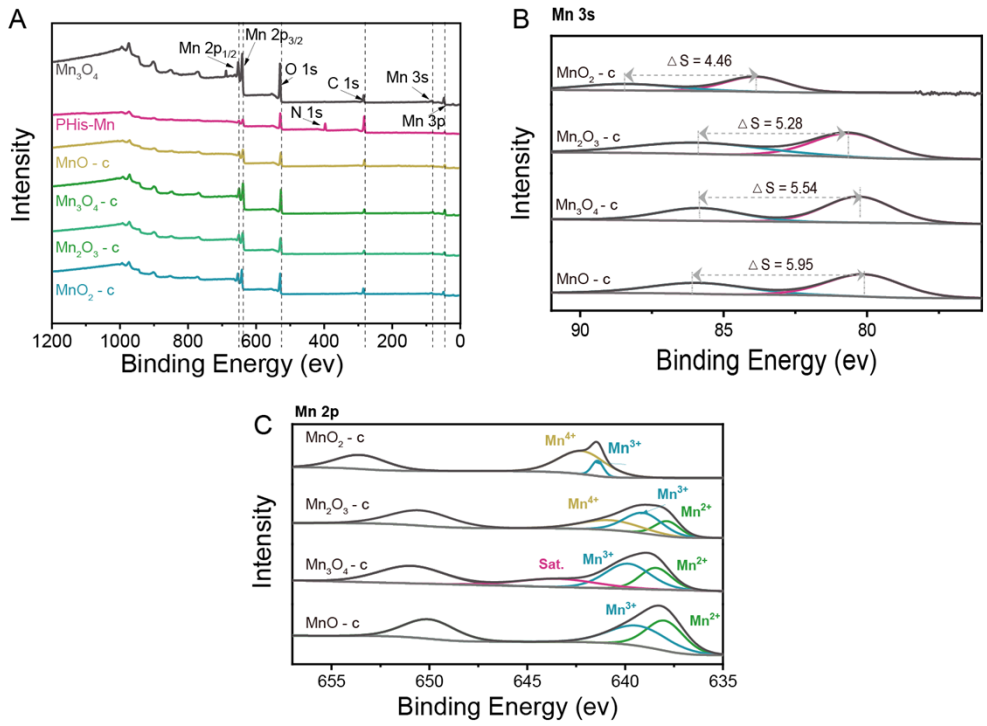

Figure S2. XPS analysis of different kind of manganese oxides (A) full spectra; (B) Mn 2p and (C) Mn 3s.

Understanding the valence of Mn could better explain the structure and catalytic performance of Mn_3O_4, XPS analysis was also used to further investigate the chemical composition and the valence of Mn. The XPS results of different manganese oxides were shown in the Figure S1C, S1D and S2. They were similar to each other, just the ratio changed between Mn^{2+}, Mn^{3+} and Mn^{4+} (Table S2), where more Mn^{3+} or Mn^{4+} were calculated in high–valence manganese reference substances. The peak around 643 eV (red) in the Mn 2p spectra was the satellite peak of Mn^{2+}.[18]

To further explore the valence of Mn_3O_4, the rank of average oxidation states (AOS) (Equation 4) was calculated: MnO_2-c (3.91) > Mn_2O_3-c (2.98) > Mn_3O_4 (2.75) > Mn_3O_4-c (2.69) > PHis-Mn (2.59) > MnO-c (2.23), which was consistent with the result of Table S2. The AOS of PHis-Mn was slightly lower than Mn_3O_4, it might be due to the fact that the imidazolyl group of PHis is an electron donating group, resulting in a slight decrease in the average valence of Mn in the oxide.[14]

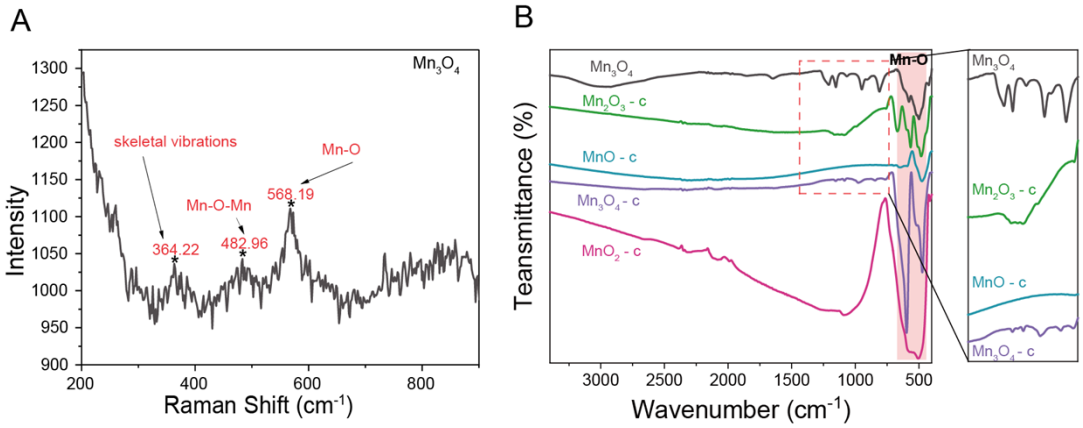

Figure S3. (A) Raman spectrum of Mn_3O_4 and (B) FT-IR spectra of different kinds of manganese oxides.

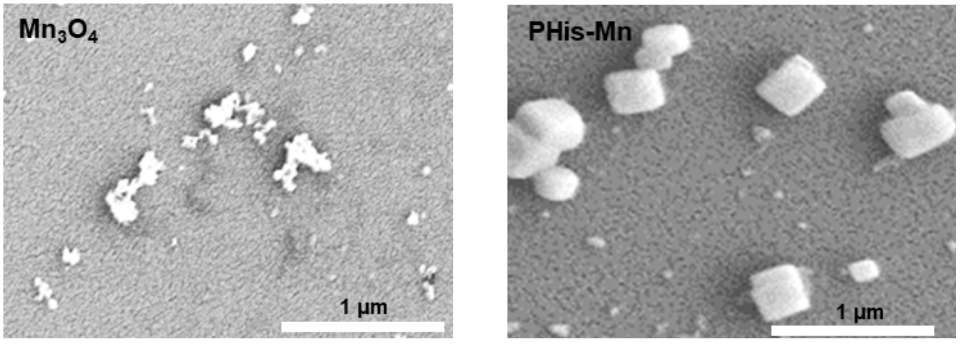

Figure S4. SEM images of Mn_3O_4 and PHis-Mn.

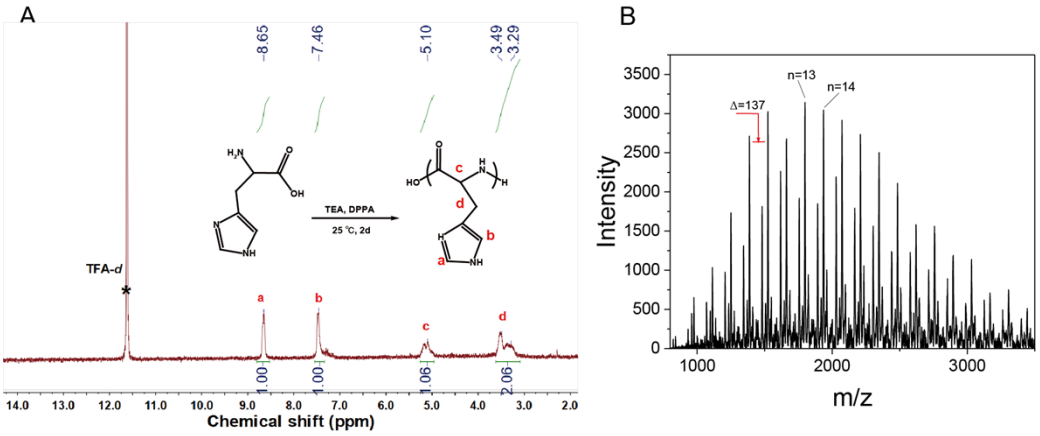

Figure S5. (A) Synthesis of PHis and ^{1}H NMR spectrum of PHis in TFA-*d*. (B) MALTI-TOF mass spectrum of PHis (n = polymerization degree).

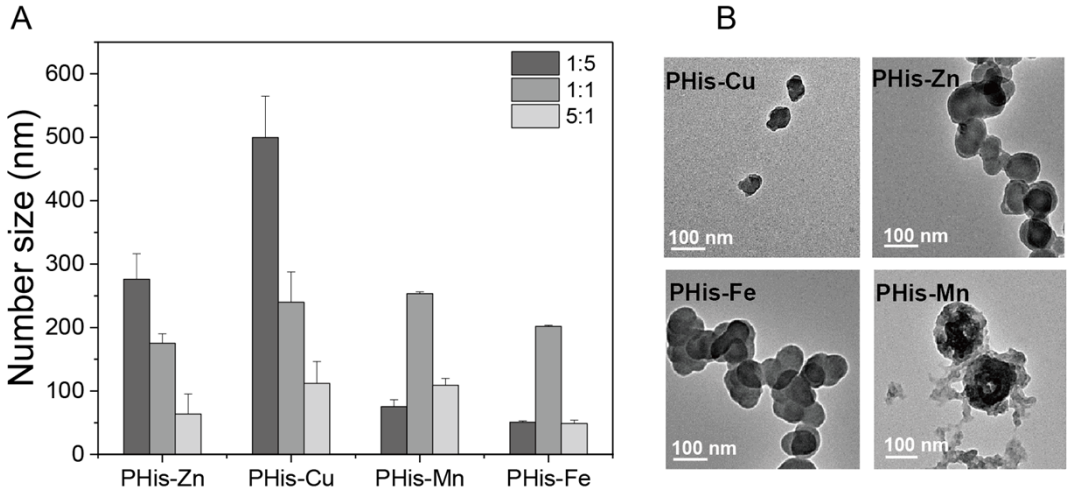

Figure S6. (A) Hydrodynamic diameters of PHis-M NPs (M = Cu, Zn, Fe, and Mn) prepared by different feeding molar ratios of His and metal ions (1:5, 1:1, and 5:1). (B) TEM images of PHis-M NPs prepared at a molar ratio of 1:1.

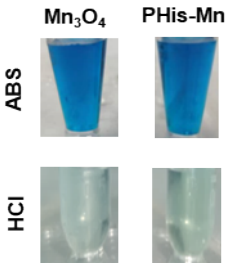

Figure S7. The comparison of oxidized performance of Mn_3O_4 and PHis-Mn (pH 5.5).

The XPS of PHis-Mn (Figure S1C and S1D) and the oxidized performance (Figure S7) demonstrated the successful preparation of PHis-coated Mn_3O_4.

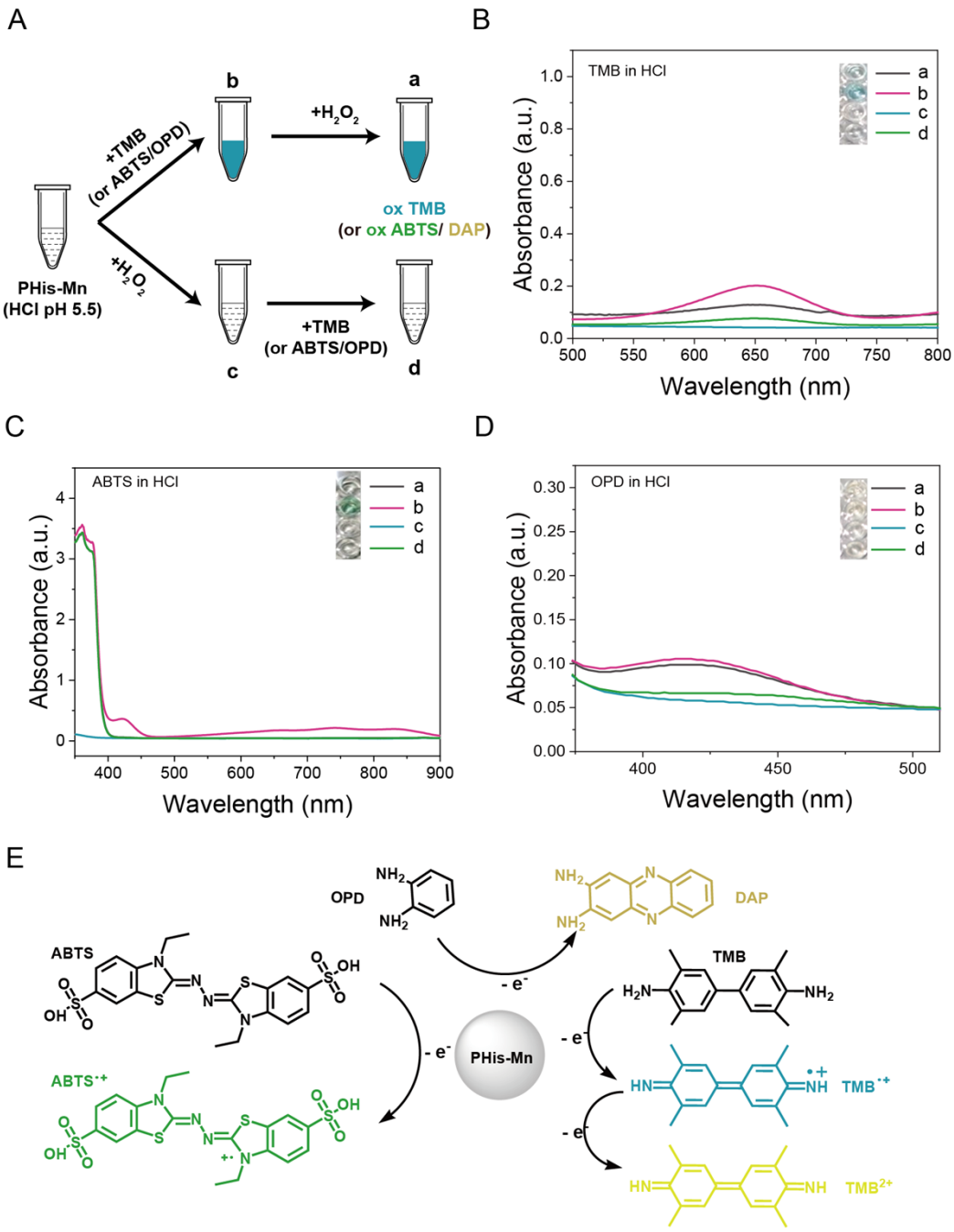

Figure S8. (A) Diagram of addition sequences of H_2O_2 and TMB (or ABTS, OPD) in Figures B-D. The enzyme-like activity of PHis-Mn (70 μg/mL) to (B) TMB (0.8 mM), (C) ABTS (3 mg/mL), (D) OPD (0.16 mM) under HCl at pH 5.5 with or without H_2O_2 (a, b, c, d correspond to the tubes in (A)). (E) Schematic illustration of the oxidation of ABTS, OPD and TMB over PHis-Mn.

Adding TMB first and then adding H_2O_2 has little effect on the catalysis (Figure 2B, S8B, curve a). If the order was exchanged, substrates were not substantially oxidized (Figure 2B and S8B, curve

d). If TMB is added firstly, it will be preferentially oxidized by PHis-Mn to ox-TMB. Otherwise, adding H_2O_2 first would decline the content of ox-TMB. There were two possible reasons: Firstly, it was that firstly added H_2O_2 would occupy the active site and inhibit the catalytic effect as explained above; secondly, H_2O_2 would change the structure of PHis-Mn, leading to the reduction of its catalytic performance. What's more, the phenomenon of substrates stronger oxidation in ABS (Figure 2B-D) than in HCl solution (Figure S8B-D).

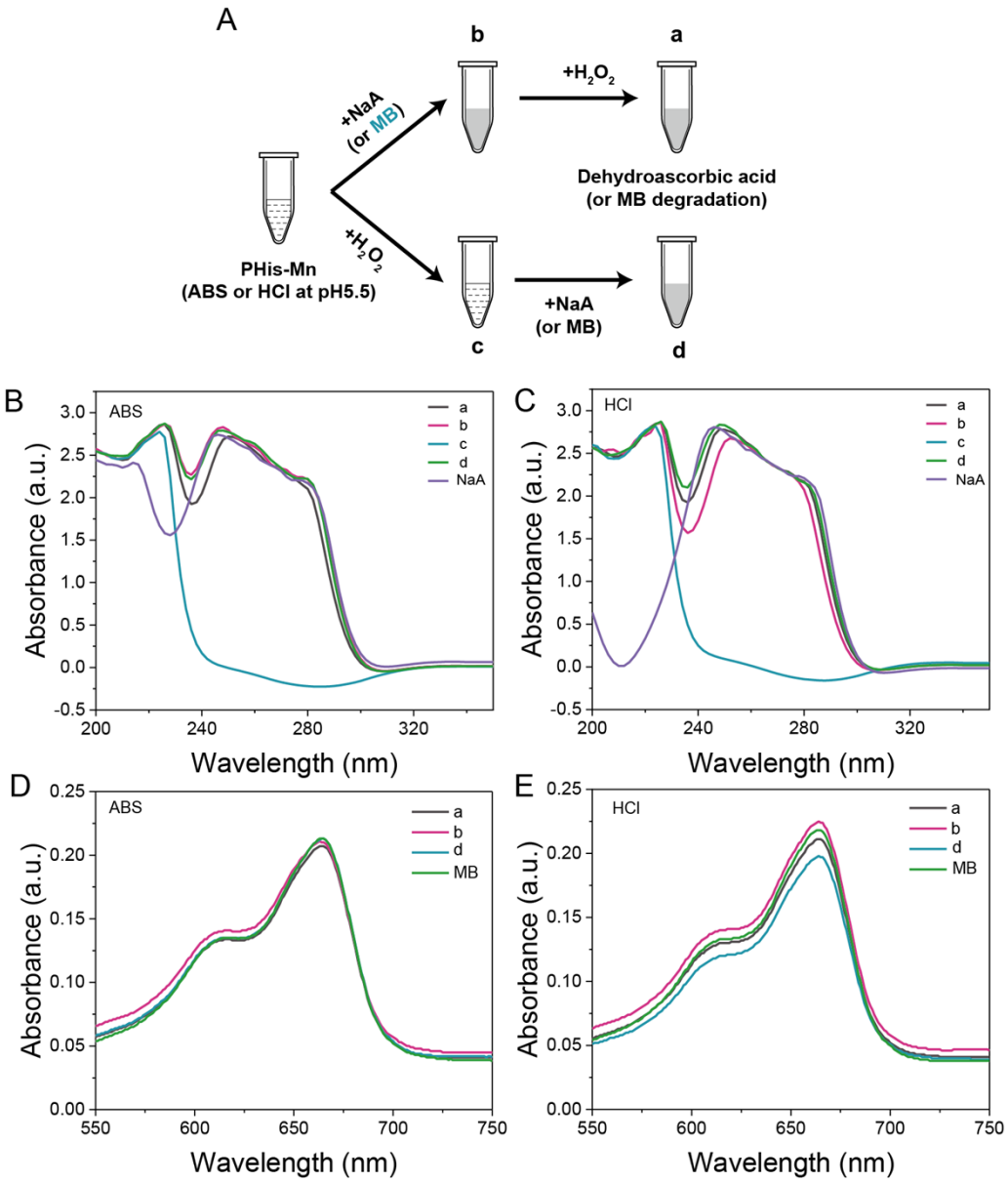

Figure S9. (A) Diagram of addition sequences of H_2O_2 and NaA or MB in (B-E). The enzyme-like activity of PHis-Mn (70 μg/mL) to (B, C) NaA (0.8 mM) and (D, E) MB (7 μg/mL) under ABS or HCl at pH 5.5 with or without H_2O_2. (a, b, c, d correspond to the tubes in (A)).

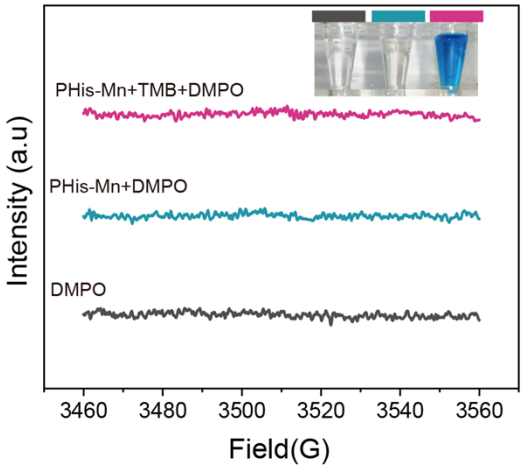

Figure S10. ROS detection by EPR spectra using DMPO as a probe.

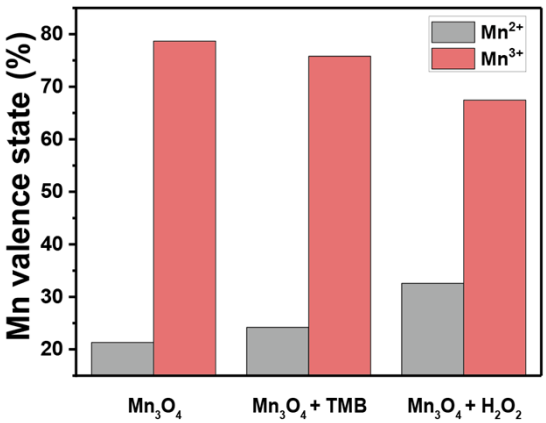

Figure S11. The quantification result of Mn^{2+}/Mn^{3+} of Mn_3O_4 after TMB or H_2O_2 treatment by analyzing the Mn 2p results in Figure 2E.

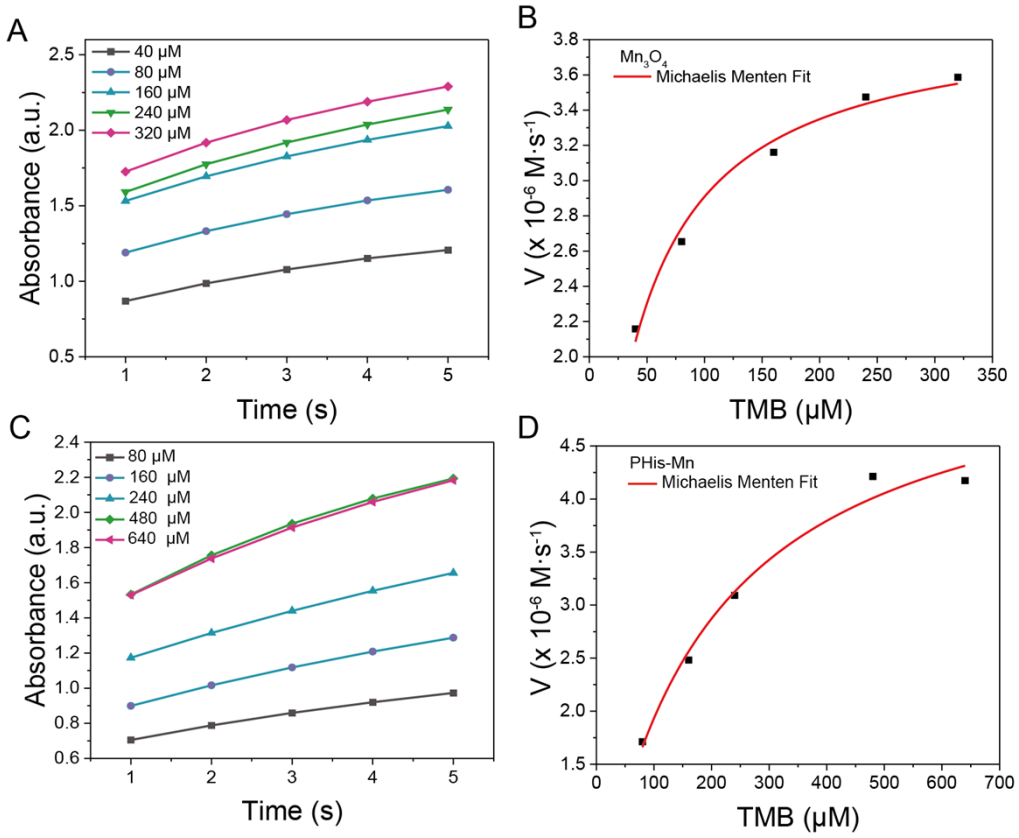

Figure S12. Evaluation of the enzymelike activity of Mn_3O_4 and PHis-Mn at ABS (pH 5.5). (A, C) Oxidation kinetics of TMB in the presence of different concentrations of TMB. (B, D) Corresponding Michaelis–Menten kinetics curves. The reactions were performed with 70 μg/mL Mn_3O_4 or PHis-Mn.

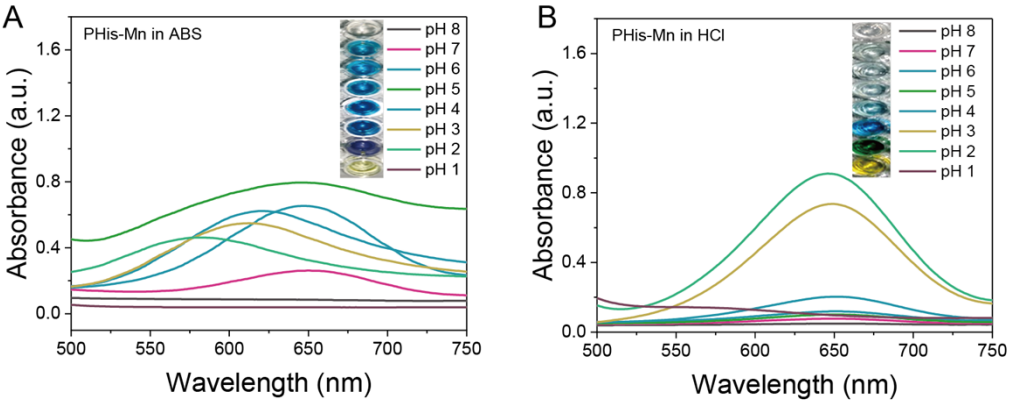

Figure S13. UV-vis absorption and typical photographs of TMB oxidation by PHis-Mn at different pH conditions in ABS (A) or HCl (B) solution (pH was tuned with HCl or NaOH).

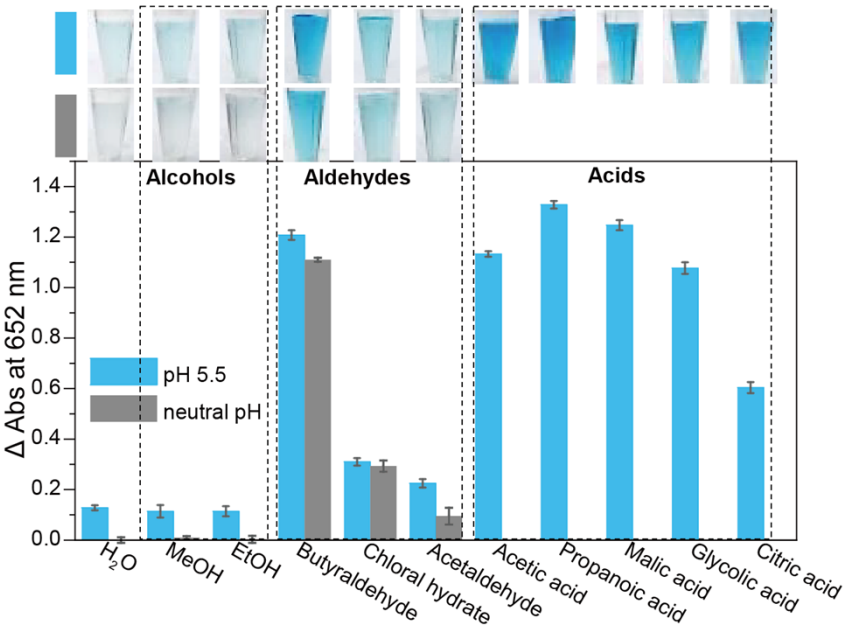

Figure S14. The effects of different kinds of alcohols, aldehydes and acids on the catalytic performance of Mn_3O_4 (Mn_3O_4: 70 μg/mL; TMB: 0.8 mM; H_2O at neutral pH as control).

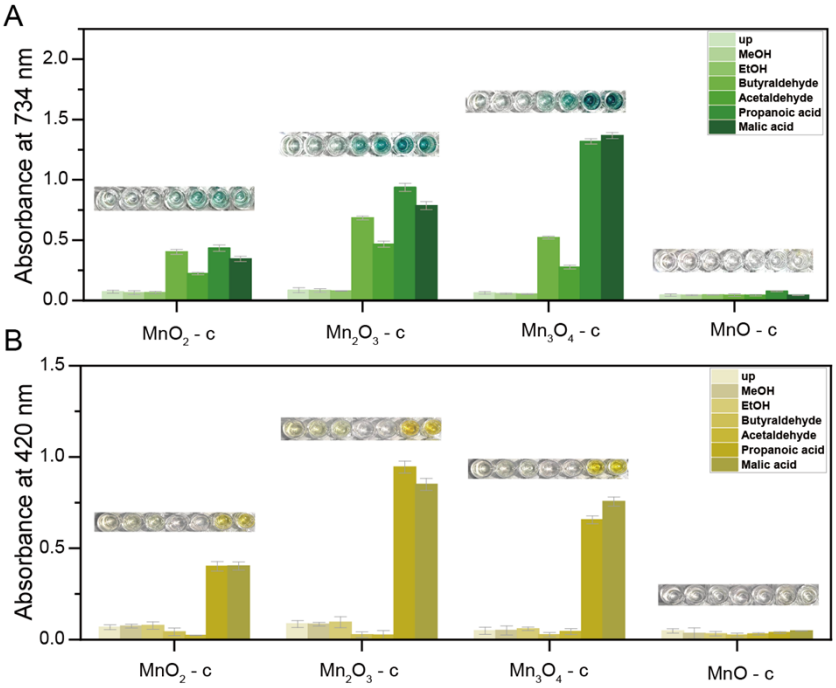

Figure S15. The effects of different kinds of aldehydes, organic acids and alcohols on the catalytic performance of ABTS or OPD by commercial manganese oxides. (Manganese oxides: 70 μg/mL; ABTS or OPD: 0.8 mM; pH 5.5)

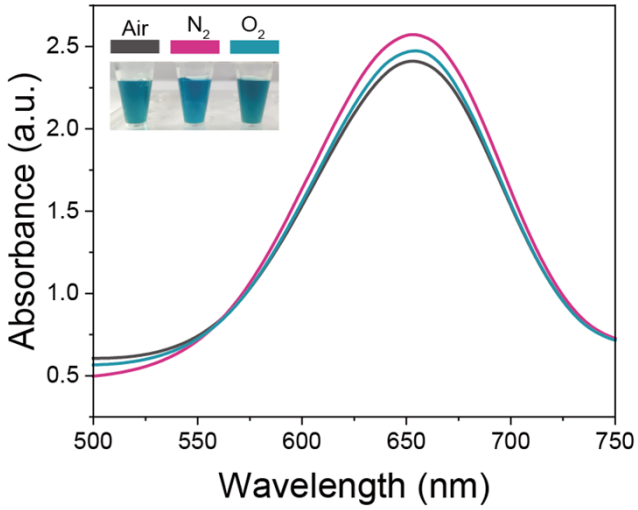

Figure S16. UV-vis absorption of TMB oxidation by PHis-Mn at pH 3 HCl solution purged with O_2, N_2 or air.

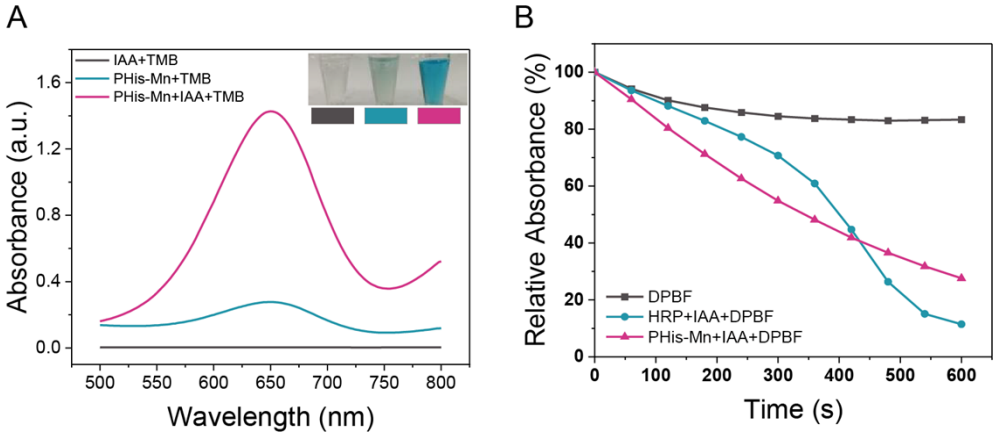

Figure S17. (A) PHis-Mn catalyzed TMB oxidation under IAA co-incubation (PHis-Mn: 70 μg/mL; IAA: 0.2 mg/mL). (B) Comparison of consumption of DPBF for HRP and PHis-Mn at the same concentration (PHis-Mn or HRP: 14 μg/mL, IAA: 500 μM; DPBF: 50 μM).

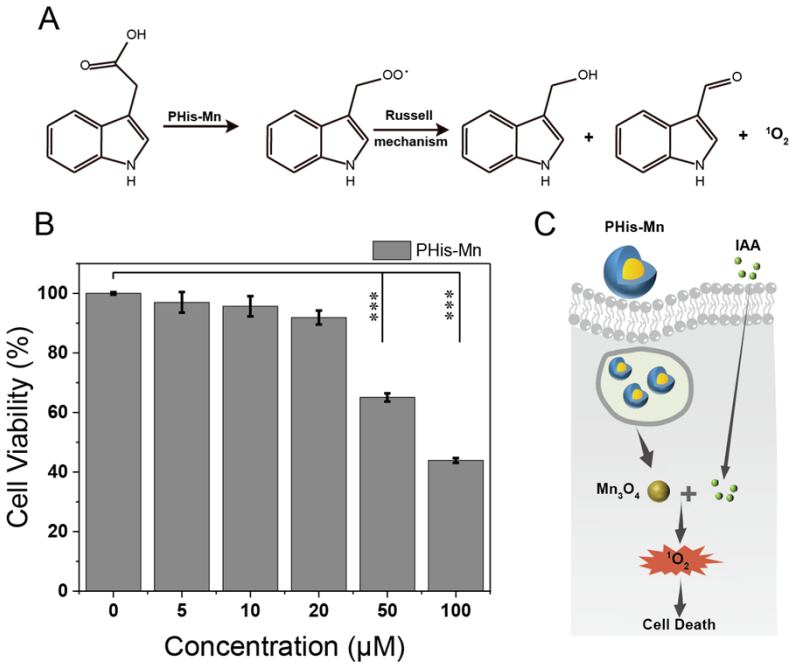

Figure S18. (A) The proposed reaction equation of the PHis-Mn catalyzed activation of IAA. (B) Cell viability of different concentration of PHis-Mn to 4T1 cells. (B) Schematic illustration of cytotoxicity of PHis-Mn catalyzed activation of IAA.

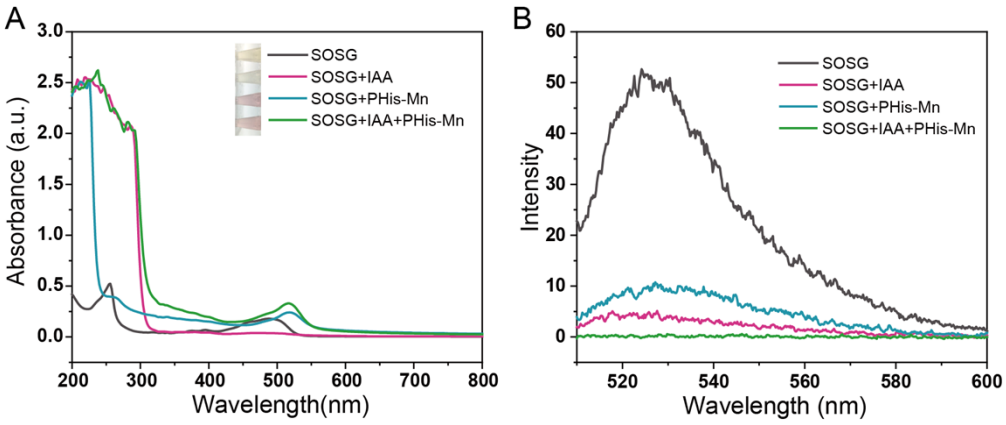

Figure S19. $^1O_2$ detection using SOSG a probe did not work in the Phis-Mn+IAA system. (A) UV-vis and (B) fluorescence results showed that after adding PHis-Mn, the UV absorption peak of SOSG redshifted and the fluorescence intensity significantly declined, indicating that the structure of the SOSG was destroyed and SOSG cannot be used to detected $^1O_2$ in this work.

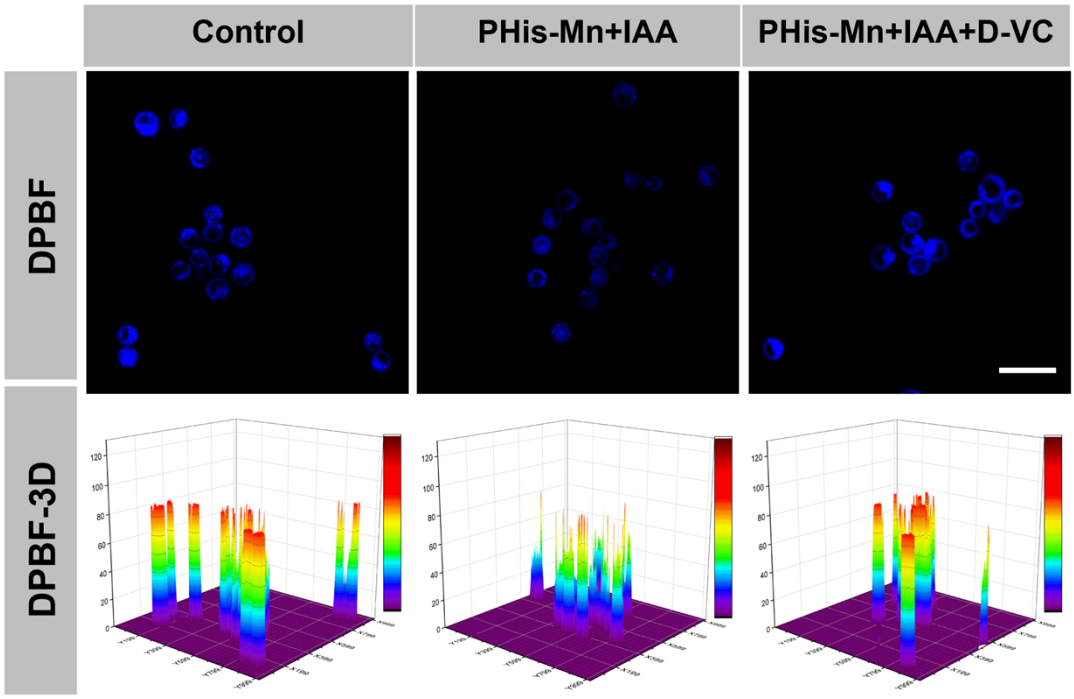

Figure S20. Confocal laser scanning microscope (CLSM) analysis of intracellular $^1O_2$ generation. Scale bar: 50 μm.

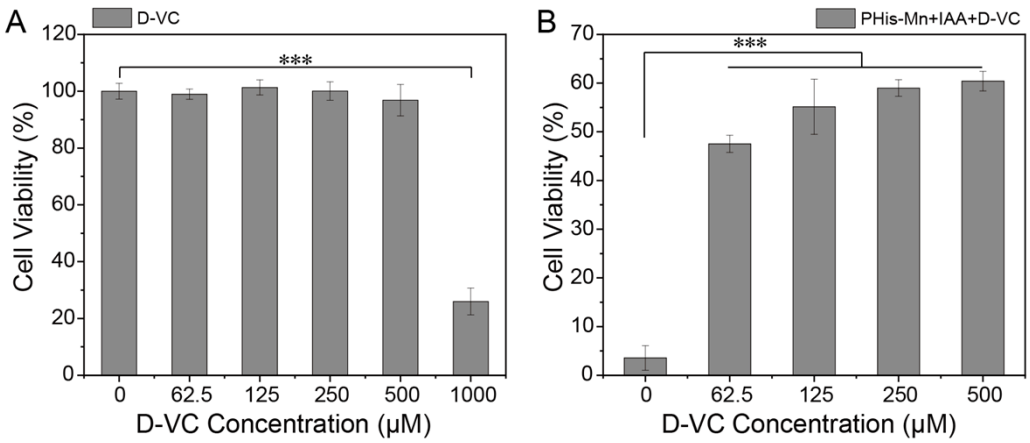

Figure S21. Cell viability analysis of 4T1 cells after incubation with different concentration of (A) D-VC and (B) PHis-Mn+IAA+D-VC. (n = 5; *** $p < 0.001$)

Table S1. Metal contents in different PHis-coated NPs determined by ICP-OES.

Material	Metal contents (wt%)
PHis-Cu	15.84
PHis-Fe	18.08
PHis-Mn	18.72
PHis-Zn	14.84

Table S2. The ratios of Mn^{2+}, Mn^{3+} and Mn^{4+} as determined by Mn 2p XPS spectra.

Samples	Mn^{2+} (%)	Mn^{3+} (%)	Mn^{4+} (%)
Mn_3O_4	21.32	78.68	-
PHis-Mn	31.14	68.86	-
MnO-c	44.39	55.61	-
Mn_2O_3-c	21.80	44.60	33.60
Mn_3O_4-c	30.38	69.62	-
MnO_2-c	-	14.06	85.94

Table S3. The optimized structures of the intermediate compounds for CH_3COOH reduction process at the surfaces of Mn_3O_4 (211) and MnO (100). The red, purple, gray and white balls represent the O, Mn, C and H atoms, respectively.

Intermediate compounds	**Mn_3O_4 (211) surface**	**MnO (100) surface**
(a) CH_3COOH*	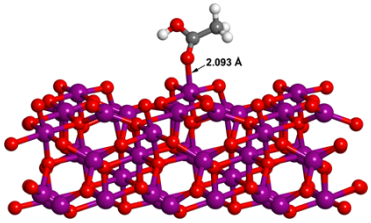	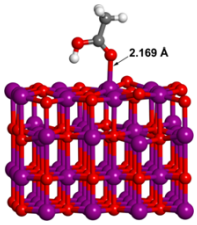
(b) CH_3CO*	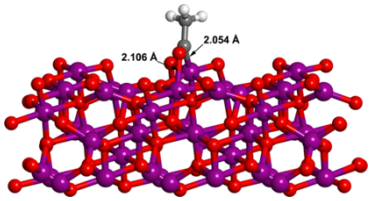	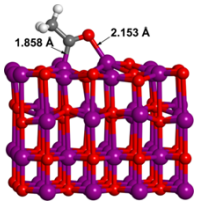
(c) CH_3CHO*	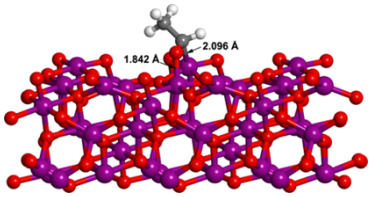	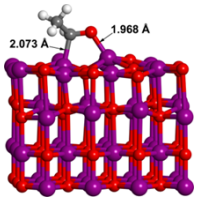
(d) CH_3CH_2O*	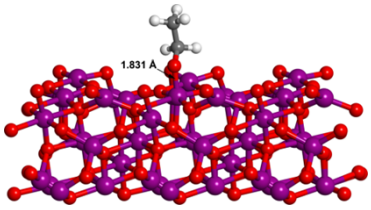	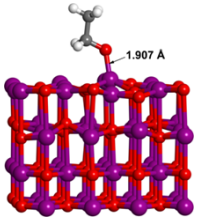
(e) CH_3CH_2OH*	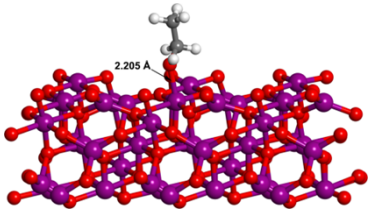	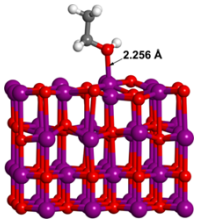

References

1. N. Nishi, T. Naruse, K. Hagiwara, B.-i. Nakajima and S. Tokura, *Makromol. Chem.*, 1991, **192**, 1799-1809.
2. Y. Pu, Y. Du, M. M. Khin, V. Ravikumar, S. A. Rice, H. Duan and M. B. Chan-Park, *Macromol Rapid Commun*, 2017, **38**, 1600601.
3. D. Patel, Y. Chang and G. H. Lee, *Current Applied Physics*, 2009, **9**, S32-S34.
4. Y. Zhao, X. Song, Z. Yin and Q. Song, *Journal of Colloid and Interface Science*, 2013, **396**, 29-38.
5. C. Gu, L. Shanshan, J. Huang, C. Shi and J. Liu, *Sensors and Actuators B: Chemical*, 2013, **177**, 453-459.
6. A. G. Karunanayake, O. A. Todd, M. Crowley, L. Ricchetti, C. U. Pittman, R. Anderson, D. Mohan and T. Mlsna, *Chemical Engineering Journal*, 2018, **331**, 480-491.
7. G. Kresse and J. Furthmüller, *Comput. Mater. Sci.*, 1996, **6**, 15-50.
8. J. P. Perdew, K. Burke and M. Ernzerhof, *Phys. Rev. Lett.*, 1996, **77**, 3865-3868.
9. P. E. Blöchl, *Physical Review B*, 1994, **50**, 17953-17979.
10. G. Kresse and D. Joubert, *Phys. Rev. B*, 1999, **59**, 1758-1775.
11. V. V. Anisimov, J. Zaanen and O. K. Andersen, *Phys. Rev. B*, 1991, **44**, 943-954.
12. A. A. Peterson, F. Abild-Pedersen, F. Studt, J. Rossmeisl and J. K. Nørskov, *Energy Environ. Sci.*, 2010, **3**, 1311-1315.
13. P. Carloni, E. Damiani, L. Greci, P. Stipa, F. Tanfani, E. Tartaglini and M. Wozniak, *Research on Chemical Intermediates*, 1993, **19**, 395-405.
14. M. Sayed, F. Xu, P. Kuang, J. Low, S. Wang, L. Zhang and J. Yu, *Nat Commun*, 2021, **12**, 4936.
15. R. Baddour-Hadjean and J.-P. Pereira-Ramos, *Chem. Rev.*, 2010, **110**, 1278-1319.
16. D. Gosztola and M. J. Weaver, *J. Electroanal.Chem.Interfacial Electrochem.*, 1989, **271**, 141-154.
17. S. Bernardini, F. Bellatreccia, A. Casanova Municchia, G. Della Ventura and A. Sodo, *J. Raman Spectrosc.*, 2019, **50**, 237-247.
18. Z. Yuan, X. Liu, J. Ling, G. Huang, J. Huang, X. Zhu, L. He and T. Chen, *Biomaterials*, 2022, **287**, 121620.